Journal of Molecular Graphics and Modelling 55 (2015) 115–122

Contents lists available at ScienceDirect

Journal of Molecular Graphics and Modelling

journal homepage: www.elsevier.com/locate/JMGM

Conformational diversity of bacterial FabH: Implications for molecular recognition specificity

Anuradha Mittal [1], Michael E. Johnson *

Center for Pharmaceutical Biotechnology, University of Illinois at Chicago, 900 S. Ashland Ave—m/c 870, Chicago, IL 60607-7173, USA

ARTICLE INFO

Article history:
Accepted 7 November 2014
Available online 15 November 2014

Keywords:
FabH
Conformational diversity
Binding specificity
Computational solvent mapping

ABSTRACT

The molecular basis of variable substrate and inhibitor specificity of the highly conserved bacterial fatty acid synthase enzyme, FabH, across different bacterial species remains poorly understood. In the current work, we explored the conformational diversity of FabH enzymes to understand the determinants of diverse interaction specificity across Gram-positive and Gram-negative bacteria. Atomistic molecular dynamics simulations reveal that FabH from *E. coli* and *E. faecalis* exhibit distinct native state conformational ensembles and dynamic behaviors. Despite strikingly similar substrate binding pockets, hot spot assessment using computational solvent mapping identified quite different favorable binding interactions between the two homologs. Our data suggest that FabH utilizes protein dynamics and seemingly minor sequence and structural differences to modulate its molecular recognition and substrate specificity across bacterial species. These insights will potentially facilitate the rational design and development of antibacterial inhibitors against FabH enzymes.

1. Introduction

The increasing resistance to available antibiotics has led to an urgent need for the discovery of novel modes of action that could be used to combat drug-resistant microbial strains. Recently, the bacterial type II fatty acid synthase (FASII) system has emerged as a promising novel antibiotic target. FASII enzymes carry out fatty acid biosynthesis and regulate the fatty acid composition of bacteria. The membrane lipid biosynthesis and its homeostasis are essential for bacterial survival [1]. The organization and structure of the bacterial FASII system is distinct from that of the mammalian multienzyme type I system, offering selective inhibition by antimicrobial agents and reduced risks of nonspecific toxicity [2,3]. Further, several natural product [4–7] and synthetic inhibitors [8,9] targeting FASII enzymes have demonstrated the validity of the FASII pathway as an antibiotic target.

β-Ketoacyl-acyl carrier protein synthase III (FabH) is an essential enzyme in the FASII pathway, which catalyzes the first step in the pathway, the condensation of acyl-CoA primers with malonyl-ACP. FabH from Gram-positive and Gram-negative bacteria are known to have distinct preferences for acyl-CoA primers. This is functionally important, as the substrate specificity of the enzyme governs the fatty acid profile of the organism [10]. FabH from *E. coli* and other Gram-negative organisms are selective for acetyl-CoA and produce straight-chain fatty acids, while the FabH enzymes of Gram-positive bacteria such as bacilli prefer branched-chain primers and produce branched-chain fatty acids. The differential ligand specificity across homologs has also been observed in FabH drug design [11]. The identified FabH inhibitors show varied inhibitory potencies for FabH from different bacterial species [11]. The origin of the observed inter-species variability of substrate and inhibitor activity is not obvious. The substrate binding cleft of FabH is predominantly lined by hydrophobic residues that form the majority of protein–ligand interactions in the co-crystal structures. A few hydrogen bonds with the polar and charged residues at the base and at the entrance of the pocket are the likely interactions that define the binding specificity in these complexes. However, the sequences and the structures of the FabH substrate-binding pockets are highly conserved across bacterial genomes. Out of the 24 residues of the FabH binding pocket that lie within 5 Å of any atom of the inhibitor in the *E. coli*

Abbreviations: CSM, computational solvent mapping; ecFabH, *Escherichia coli* FabH; efFabH, *Enterococcus faecalis* FabH; FAB, fatty acid biosynthesis; FAS, fatty acid synthase; MD, molecular dynamics; MM-GBSA, molecular mechanics-generalized born surface area; PDB, Protein Data Bank; RMSD, root mean squared deviation.

* Corresponding author. Tel.: +1 312 996 9114; fax: +1 312 431 9303.
E-mail address: mjohnson@uic.edu (M.E. Johnson).
[1] Present address: Department of Biomedical Engineering and Center for Biological Systems Engineering, Washington University in St. Louis, MO 63112, USA.

http://dx.doi.org/10.1016/j.jmgm.2014.11.004
1093-3263/

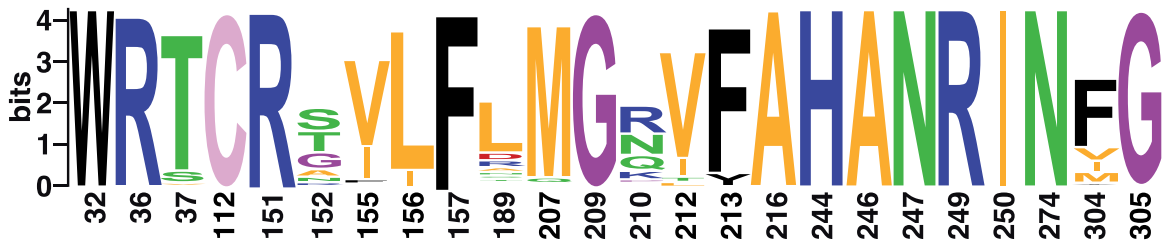

Fig. 1. *Conservation of FabH binding pocket residues represented by sequence logo.* Residues are colored according to their physico-chemical properties. The logo was generated by aligning 358 bacterial FabH sequences identified from UniProt. Multiple sequence alignments were generated with ClustalW [29] using Jalview version 2 [30,31] and the sequence logo was generated with WebLogo version 2.8.2 [32].

inhibitor-bound structure (PDB: 1MZS), 14 residues are strictly conserved and 8 show conservation of their physico-chemical properties across bacterial species (Fig. 1). Since the shape and the chemical complementarity of the binding interfaces are the primary determinants of the specificity of interaction, the mechanism for substrate specificity in the highly conserved FabH enzyme remains elusive.

Proteins exist as dynamic ensembles of conformational substates, and the relative population of these states and the transitions between them regulate their intermolecular interactions [12,13]. The subtle differences in amino acid residues within and around the binding pocket can potentially modulate the thermally accessible conformational substates populated by different homologs. Gajiwala et al. reported the presence of diverse rotameric states of the acyl-CoA binding site residues in the crystal structures of FabH enzymes from multiple species and suggested that the minor differences in the architecture of the FabH active site modulate the enzyme's substrate specificity [14]. The crystal structures, however, report only the highly populated regions on the free energy landscape corresponding to the global minimum or the minimum under the crystallization conditions and may not adequately represent the functionally relevant configurational diversity. Furthermore, the atomistic molecular dynamics (MD) simulations of *E. coli* FabH reported in a recent study show significant heterogeneity in the conformational ensemble of both the ligand bound and unbound forms [15]. Thus, the observed conformational diversity in the experimental data may not entirely account for the enzyme's varied substrate specificity. In this work we carried out an in-depth exploration of the structural flexibility and equilibrium conformational ensemble of FabH from a Gram-positive and a Gram-negative bacterium to understand the implications of minor sequence variations on molecular recognition.

Based on the availability of the crystal structures, we used FabH from *Escherichia coli* (ecFabH) and *Enterococcus faecalis* (efFabH) as model systems to investigate the determinants of recognition specificity in Gram-negative and Gram-positive bacteria, respectively. The two sequences show a sequence identity of 39% and a sequence similarity of 56% (Fig. S1). Nineteen of the 24 binding pocket residues are conserved in the two sequences. We used atomistic molecular dynamics (MD) simulations to characterize the conformational space accessible to the two homologs under native conditions. We then focused our analysis on the ligand binding properties of the conformational ensembles of the two homologs. To identify consensus favorable binding sites across diverse conformations from ecFabH and efFabH ensembles, we used an approach similar to the computational solvent mapping (CSM) protocol initially introduced by Vajda et al. [16] and Carlson et al. [17,18]. Interestingly, our data suggest that despite high sequence similarity, ecFabH and efFabH show markedly differing conformational preferences and distinct CSM identified hot spots, providing potential explanation for varied ligand specificities seen among FabH enzymes.

2. Materials and methods

2.1. Molecular dynamics simulations

The crystal structures of FabH from *E. coli* (PDB: 1MZS [19]) and *E. faecalis* (PDB: 3IL5 [14]) were used as the starting structures for the simulations. The ecFabH structure is complexed with an indole analog exhibiting an IC_{50} value of 7 μM. The efFabH structure is complexed with a benzoylamino-benzoic acid derivative exhibiting an IC_{50} value of 1.6 μM. For each structure two simulations of the dimeric form of FabH were carried out, with (bound) and without (holo) the bound ligand. The structure preparation was done using the Sybyl 8.1 suite (Tripos, Inc.). The MD simulations were performed using the PMEMD module of the Molecular Dynamics Package AMBER11 [20] and the AMBER03 forcefield [21]. The protein structures were solvated in a 100 Å cubic waterbox (TIP3P). Chloride ions were added to replace water molecules in the box to neutralize the system. Periodic boundary conditions were applied with a 10 Å nonbonded cutoff. For all MD simulations, the system was first subjected to a steepest decent energy minimization followed by a conjugate gradient minimization. First, only the water molecules around the protein were minimized for 5000 steps followed by the minimization of the entire system for another 5000 steps. The system was then heated from 0 K to 300 K using canonical (NVT) ensemble for 30 ps. Finally, 50 ns production runs were carried out at 300 K, the first 10 ns of which were discarded as equilibration time. For the ligand-bound simulations the partial charges on the ligands were assigned using the restrained electrostatic potential fit (RESP) model with the Gaussian 03 program [22]. The Antechamber program was used to generate the topology and parameter files for the ligands using the General Amber Force Field (GAFF).

The choice of the 50 ns simulation length was based on the comparative analysis of the various FabH crystal structures available in the PDB. The available structural data do not suggest any large scale domain movements (Fig. S2A) and mainly reflect side chain flexibility, which can usually be sampled in ps–ns timescale. The average pairwise RMSD between the available eighteen structures was found to be 0.74 Å (Fig. S2A). Fig. S2B shows the backbone RMSDs of the apo and bound forms of ecFabH and efFabH as a function of time indicating that both systems converged within a few nanoseconds.

The trajectories were postprocessed and analyzed using the ptraj module of the AMBER11 package. For hydrogen bond propensity calculations, the hydrogen bonds were identified using the cutoff criteria of a maximum distance between the hydrogen bond donor and acceptor atom of 3.5 Å and donor–hydrogen–acceptor angles in the range 90°–180°. Unless otherwise specified, the FabH residues mentioned in the text correspond to the residue numbering in the 1MZS PDB file. The residue numbering used for PDB file 3IL5 was derived after renumbering the residues in the structure file according to the alignment using the 1MZS structure.

2.2. Computational solvent mapping

Computational solvent mapping was applied to the ecFabH (PDB: 1MZS) and to the efFabH (PDB: 3IL5) structures. The snapshots generated from the last 40 ns MD simulation of the holo forms were clustered based on the active site pocket heavy atom RMSD from the respective solved crystal structures. The *K*-means clustering algorithm in the MMTSB toolset [22] was used for clustering. The binding pocket residues considered for RMSD clustering were: 32–39, 111–113, 150–157, 187–190, 207–220, 243–251, 274 and 303–306. A clustering radius of 2 Å yielded 18 clusters for ecFabH and 10 clusters for efFabH. Finally, the snapshots corresponding to the centroid of each cluster were selected for the CSM protocol. Five diverse organic functional groups were selected as probes—benzene for aromatic interactions; ethane for hydrophobic interactions; and methanol, methyl ammonium and acetate for hydrogen bonding interactions. For each snapshot, 100 docking trials were carried out for each probe type using 10,000 iterations of Monte Carlo simulated annealing with Autodock v4.0 [23]. The final docked poses were clustered and the best scoring conformation of each cluster for each probe type was retained as the parent molecule for that cluster. On aligning parent molecules of a particular probe type for all snapshots, consensus clusters (consisting of at least 5 parent probes) were formed. The center point of each cluster was computed from the center averages of the parent molecules of each cluster. The radius of each cluster was computed from the average deviation of parent probe centers forming a cluster from the cluster center.

2.3. Binding free energy decomposition analysis

The per-residue free energy decomposition was performed using the MM-GBSA method [24,25] integrated in AMBER11. Since the simulations of the holo and the bound structures did not suggest large structural changes upon ligand binding, we employed the single trajectory approach. The energy components were calculated using 256 snapshots extracted from the last 40 ns trajectory of the complex. The binding free energy between the inhibitor and the FabH enzyme was calculated as:

$$\Delta G_{\text{bind}} = \Delta G_{\text{complex}} - \left[\Delta G_{\text{protein}} + \Delta G_{\text{inhibitor}}\right]$$

where $\Delta G_{\text{complex}}$, $\Delta G_{\text{protein}}$ and $\Delta G_{\text{inhibitor}}$ are the free energies of the complex, the protein and the inhibitor, respectively. Each of them can be estimated according to the following equations:

$$\Delta G = \Delta G_{\text{MM}} + \Delta G_{\text{solv}} - T\Delta S$$

$$\Delta G_{\text{MM}} = \Delta G_{\text{ele}} + \Delta G_{\text{vdw}}$$

$$\Delta G_{\text{solv}} = \Delta G_{\text{PB}} + \Delta G_{\text{nonpol}}$$

where ΔG_{MM} is the molecular mechanics energy comprising the electrostatic term (ΔG_{ele}) and the van der Waals term (ΔG_{vdw});ΔG_{solv} is the solvation energy consisting of the polar contribution (ΔG_{PB}) to solvation and the nonpolar solvation term (ΔG_{nonpol}). The polar component of solvation energy was calculated using the generalized Born (GB) method in a continuum model of the solvent, and the nonpolar term was estimated by the solvent accessibility surface area method. The entropic contribution ($T\Delta S$) was not computed primarily because its calculation is highly computationally demanding and is still prone to errors [26,27]. Moreover, this simplification seems appropriate as the focus of the energetic analysis was on identifying the residues that play a dominant role in stabilizing the bound complex and not on the calculation of absolute binding free energies. Our simulation data does not show significant differences in the conformational properties between the bound and the unbound structures, so that the entropic contributions can be ignored for obtaining relative contributions of all residues to the binding [28]. The MM-GBSA decomposition process gave the van der Waals, electrostatic, polar solvation, and nonpolar solvation contributions of each inhibitor–residue pair.

3. Results and discussion

3.1. Comparison of conformational characteristics of ecFabH and efFabH

We compared the native state conformational ensembles of the two representative structures of FabH, modeled using multi-nanosecond atomistic MD simulations. We simulated the structures in holo and ligand-bound forms to assess the effects of ligand binding on protein dynamics. Despite a high level of sequence conservation, ecFabH and efFabH show different dynamic and structural behaviors. Fig. 2A and C compare the backbone and sidechain per-residue root-mean-square deviation (RMSD) profiles for the holo and the bound forms of the two structures averaged over the entire simulation. The two homologs show marked differences in the average RMSD curves. The RMSD values of the binding pocket residues are compared in Fig. 2B and D. The binding pocket residues are not tightly packed (average RMSDs are greater than 1 Å) and show distinct fluctuations between the two homologs. Notably, residues W33, R37, R151 and F219 exhibit higher conformational flexibility in efFabH (Fig. 2D) compared to the comparable residues (W32, R36, R151 and F213) in ecFabH (Fig. 2B). To evaluate the structural similarity between the ecFabH and efFabH conformational ensembles, we compared the configurations sampled by the side chains of the equivalent binding pocket residues in the two structures. The side chain torsion $\chi1/\chi2$ distributions shown in Fig. 3 reveal that residues R36, R151, L189, F213, H244, I250 and F304 populate distinct configurations in ecFabH and efFabH ensembles. In particular, different configurations of the buried residues H244, I250 and F304 between the homologous structures warrant attention as they can influence the packing of the residues around the binding pocket. Alternate side chain rotamers of F304 have been previously reported in several crystal structures of FabH from Gram-positive and -negative bacteria [14].

Fig. 2 also indicates that in ecFabH, all binding pocket residues show similar fluctuations in unbound and bound states. In efFabH, except for the residues W33, C112 and F219, which show some differences, the other binding pocket residues show similar fluctuations in unbound and bound states. However, in both homologous structures, the preferred orientations of the side chains of the binding pocket residues in the holo and bound forms significantly overlap with each other (Fig. 3). These results suggest that ligand binding does not induce large conformational changes or have profound effects on the intrinsic dynamic properties of the protein. Also, it is worth noting that the holo simulations are able to sample conformations close to the bound form, highlighting the convergence of MD simulations. To further assess the adequacy of the simulation data, we overlaid the sidechain dihedral angles derived from available FabH crystal structures (with resolution of 2.5 Å or better) on the modeled torsion distributions. The predictions from MD simulations agree reasonably well with the experimental conformations as illustrated in Fig. 3.

3.2. Analysis of protein–ligand interactions in ecFabH and efFabH co-crystal structures

The ecFabH and efFabH complexes with the bound indole analog inhibitor (PDB: 1MZS) and the benzoylamino-benzoic acid derivative (PDB: 3IL5), respectively, reveal similar binding modes of the

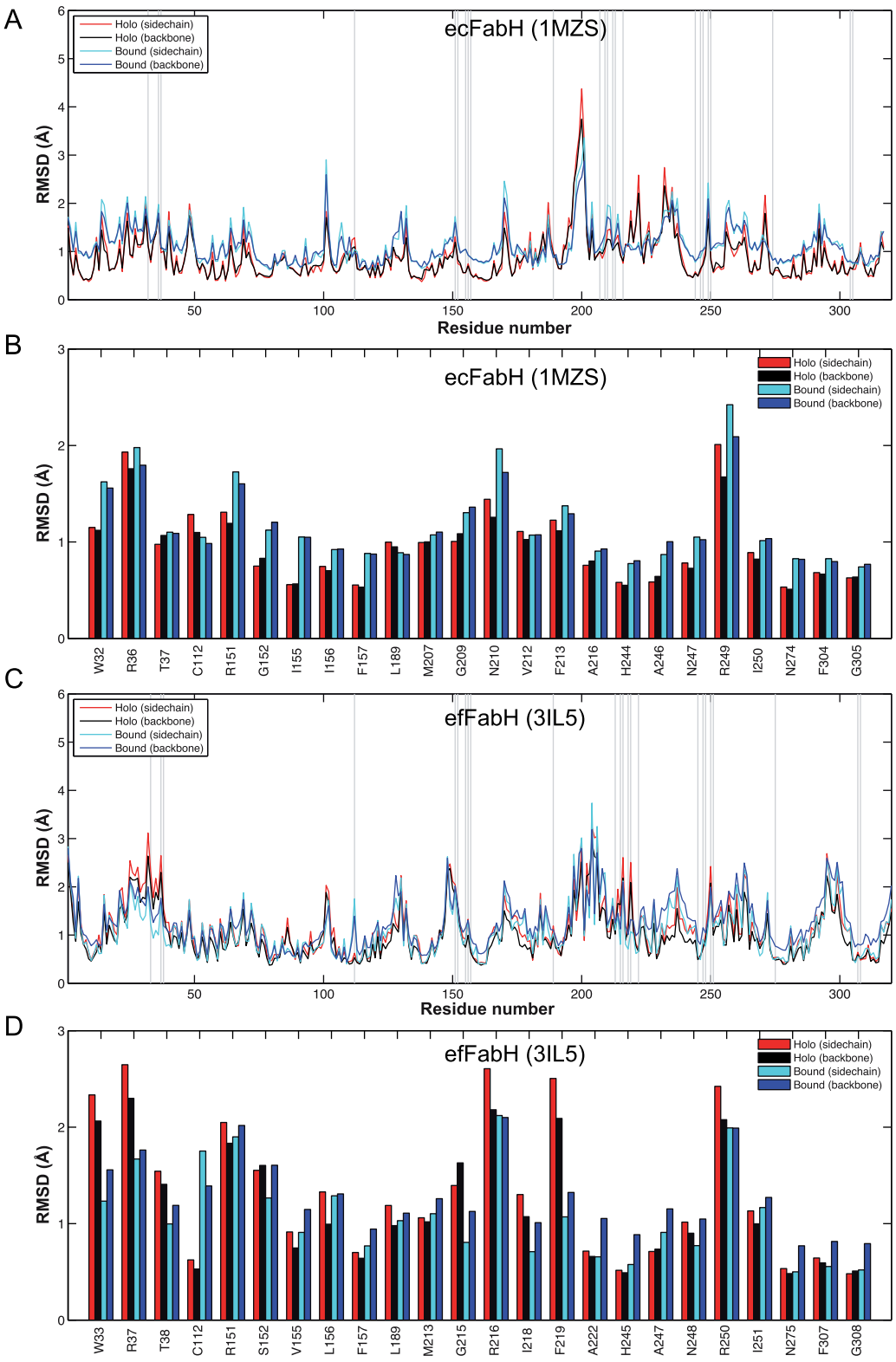

Fig. 2. *Backbone and sidechain fluctuations in ecFabH and efFabH.* (A) Average per-residue backbone and sidechain RMSD of ecFabH from the MD simulation of holo and ligand-bound forms of the 1MZS structure. (B) RMSD of the binding pocket residues in the ecFabH structure. (C) Average per-residue backbone and sidechain RMSD of efFabH from the MD simulation of holo and ligand-bound forms of the 3IL5 structure. (D) RMSD of the binding pocket residues in the efFabH structure. Grey regions in panels A and C correspond to the residues forming the binding pocket.

compounds. The inhibitors make extensive interactions with the residues lining the hydrophobic tunnel of FabH. Alanine scanning and other mutagenic studies have established that often only a few interactions within the large protein–ligand binding interfaces observed in the static crystal structures are critical for ligand binding. We therefore carried out an in-depth dynamic and energetic analysis to identify the amino acids making dominant contributions to FabH-inhibitor binding affinity. The hydrogen bonding

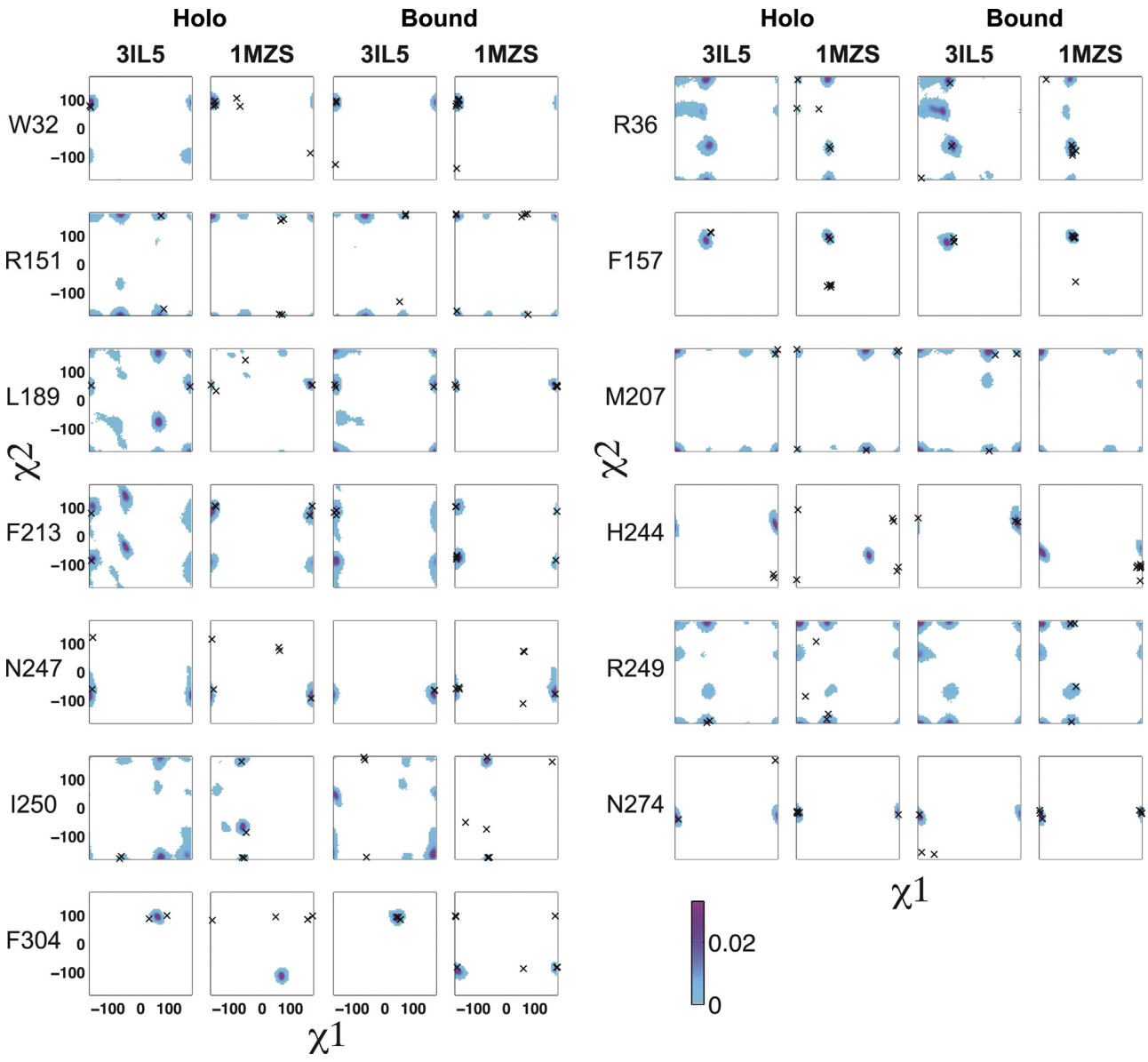

Fig. 3. *Side chain configurational properties of binding pocket residues.* The 2D distribution of torsion angles $\chi 1$ and $\chi 2$ sampled in MD simulations are plotted for conserved binding pocket residues. The color scale goes from cyan to pink, from low to high propensity. The distributions are generated using a bin width of 5°. The torsion angles observed in experimental crystal structures are indicated with black crosses "x".

propensities were calculated as the fraction of conformations showing hydrogen bonds along the MD trajectory. To quantify the energetic contributions of the individual binding pocket residues to the overall binding affinity, the per-residue free energy decomposition analysis was carried out.

The orientation of the inhibitor in the ecFabH co-crystal structure is defined by the hydrogen bonding interactions with the residues R151 and N247. The N247-inhibitor interaction was stable during the MD simulation, showing a hydrogen bond propensity of 57%. However, owing to the high flexibility of the R151 side chain (Fig. 2), the hydrogen bond between R151 and the inhibitor frequently broke and reformed during the trajectory showing a hydrogen bond propensity of 15%. In addition, transient non-native hydrogen bonds between the inhibitor and the amino acid residues R36 and N210 with propensities 40% and 25%, respectively, were observed in the course of MD simulation. Other intermolecular interactions in the co-crystal structure include the hydrophobic interactions between the 2,6-dichlorobenzyl group of the inhibitor and the residues C112, V212, A216, A246, I250 and F304; and between the indole ring of the inhibitor and the residues T37, I156, M207, G209 and F213. The remainder of the inhibitor makes additional van der Waals interactions with the residues W32, R36 and G152. The residues making a significant contribution (more than 1 kcal mol^{-1}) to the binding free energy (ΔG_{bind}) in the bound complex are summarized in the top panel of Fig. 4. The dominant contribution comes from the binding interface residues R36, R151, G152, I156, M207, G209, V212, F213, A246, N247, I250, N274 and F304. The interactions of the inhibitor with residues W32, T37, C112 and A216 as seen in the co-crystal complex do not show a significant contribution toward the binding affinity in the energetic analysis. Further decomposition into contributions from van der Waals and coulombic interactions show that the side chains of the residues R36, R151 and N247 make favorable electrostatic contributions to the binding free energy, suggesting that the hydrogen bonding interactions observed in the crystal structure and MD simulations are indeed energetically important.

In the efFabH co-crystal structure, the benzoic acid group of the inhibitor reaches deep into the pocket, making interactions

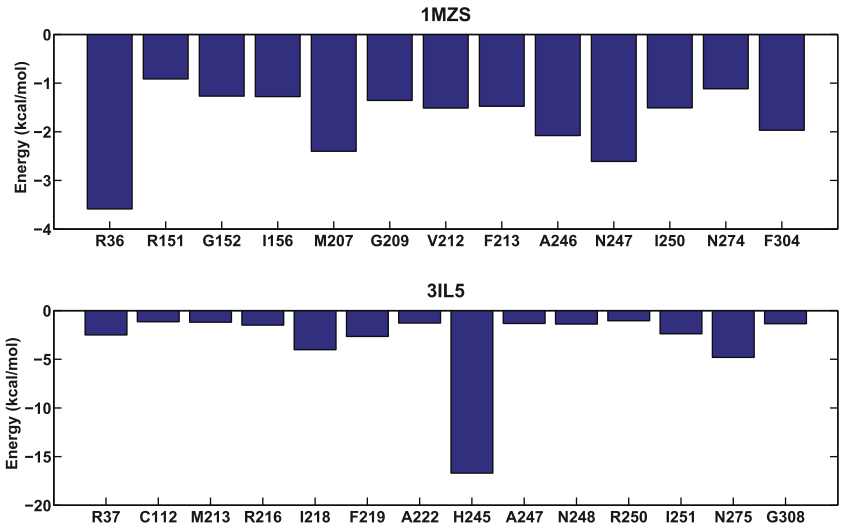

Fig. 4. *Decomposition of binding free energy on a per-residue basis.* The residues for which ΔG_{bind} is more than 1 kcal mol^{-1} are shown.

with the residues C112, I218, H245, A247, N275, F307 and G308. The benzoylamino group and the diethyl-sulfonamide portion of the inhibitor make interactions with the residues R37, L156, G215, R216, F219, N248, R250 and I251. The orientation of the compound is defined by ionic interactions between the imidazole side chain of H245 and the carboxylate oxygen of the inhibitor, and additional hydrogen bonding interactions with H245 and N275. Both of the native hydrogen bonds and ionic interaction with H245 were found to be well-maintained throughout the MD simulation. In addition, transient non-native hydrogen bonds between the inhibitor and the amino acid residues R216 and F219 were observed in the course of MD simulation. As shown in the bottom panel of Fig. 4, the overall contribution to ΔG_{bind} is dominated by the interactions with residues R37, C112, M213, R216, I218, F219, A222, H245, A247, N248, R250, I251, N275 and G308. Not surprisingly, H245 makes significantly favorable contribution to the binding free energy on account of stable electrostatic interactions with the inhibitor. The net contribution of N275 to binding also agrees with the stable hydrogen bond interactions with the inhibitor observed in the simulations. On the contrary, residues L156, G215 and F307 that make van der Waals interactions with the inhibitor in the co-crystal structure were found to be energetically insignificant in our study.

These results show that, while the binding of the two inhibitors involve the same interface, some of the key interactions differ between the two homologs. The residues involved in hydrogen bonding partners differ for both compounds. In addition, the interactions with residues C112, A222, H245, R250 and G308 are crucial for ligand binding in the co-crystal structure of efFabH, but do not show a significant contribution in the ecFabH co-crystal structure. Conversely, the contact between the bound ligand and the amino acids R151, G209 and F304 are important in ecFabH structure, but not in efFabH. It is possible that the observed differences in the favorable binding sites in the two structures are an outcome of binding to two distinct ligands. Hence, we applied a computational solvent mapping protocol for the robust identification of binding hot spots.

3.3. Hot spot analysis of ecFabH

We applied the computational solvent mapping protocol for an exhaustive exploration of favorable binding positions in the ecFabH and efFabH substrate binding pockets. Mapping was performed on the holo form of the proteins to avoid any biases from the ligand-induced conformational changes in the binding pocket. Mapping of the ecFabH structure revealed eleven conserved sites (Fig. 5A). A methyl ammonium populated cluster (ME2) located near the mouth of the pocket makes contact with the backbone of residue M207. Two acetate clusters (AC1 and AC2) interact with the backbone and the side chain of R36, respectively, and were classified as hydrogen bond acceptor consensus sites. A hydrogen bond donor site (OL2) was identified by the methanol populated cluster making contact with the side chain of N247. Two hydrogen bond donor sites were identified at the base of the pocket by a methyl ammonium cluster making contacts with the backbone of H244 (ME1) and a methanol cluster making contacts with the backbone of N247 (OL1). Docking benzene probes identified four aromatic consensus clusters. Two highly populated clusters (BE3 and BE4) were found near the mouth of the pocket making contacts with residues M207, G209, V212, F213, and I250; and W32, G152, I155 and I156, respectively. Another benzene populated region (BE1) was found at the base of the binding tunnel close to residues A216, L220, A246 and F304; and a fourth cluster (BE2) was found close to residues F157, L189, M207 and A246. Docking ethane probes identified one hydrophobic consensus cluster (ET1) interacting with residues L220, H244, A246, I251 and F304 at the base of the pocket.

To test these predictions we compared the CSM identified consensus sites with the energetically important intermolecular interactions in the inhibitor-bound ecFabH structure. The binding conformation of the indole analog in the co-crystal structure mapped onto three hot spots revealed from the CSM analysis. Of the two hydrogen bonds observed in the co-crystal structure, only the interaction with the side chain of N247 overlapped with a cluster (OL2) identified by CSM. The inhibitor-N247 interaction is also stable in the MD simulation and is predicted to contribute favorably to inhibitor binding in the energetic analysis. We did not detect any consensus probe cluster in the CSM analysis corresponding to the hydrogen bond involving R151 present in the crystal structure. Since R151 is present at the entrance of the binding pocket and is solvent exposed, it is likely that its side chain readily interchanges hydrogen bonds with the inhibitor and water molecules. The inhibitor-R151 hydrogen bond was also found to be only transiently stable in the MD simulation. The residue, however, showed favorable energy contribution in the free energy analysis. This overestimation seems to originate from insufficient conformational sampling of the residue in the snapshots used for the energetic analysis. The other two hot spots that overlapped with the bound ligand correspond to the benzene populated clusters BE1 and BE3. The BE1 site overlaps with the 2,6-dichlorobenzyl group

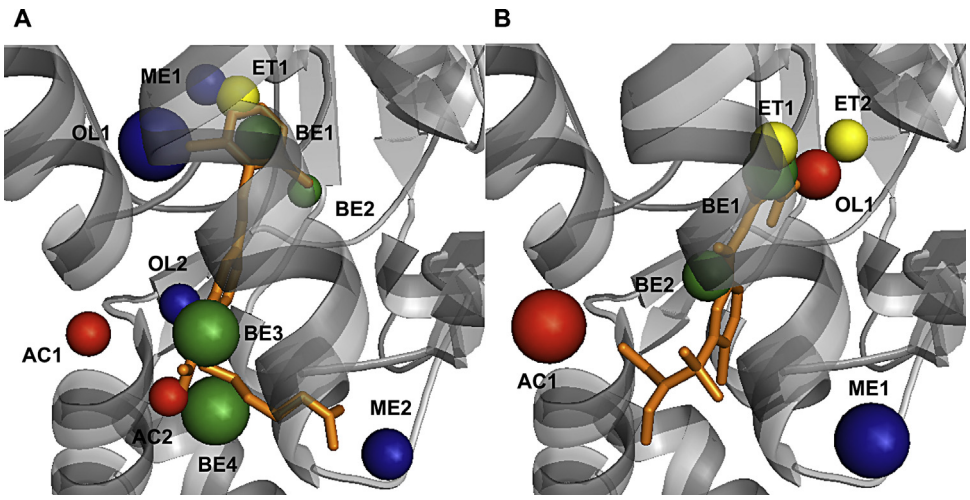

Fig. 5. *Hot spot maps of ecFabH and efFabH.* (A) Location of putative hot spots identified in ecFabH. (B) Location of putative hot spots identified in efFabH. The hot spots in panels A and B are superimposed onto crystal structure 1MZS for reference. The protein is shown in cartoon. The co-crystallized ligands are shown in stick representation. The hot spots are colored as follows: hydrogen bond donor sites: blue, hydrogen bond acceptor sites: red, aromatic sites: green, and hydrophobic sites: yellow. (For interpretation of the references to color in this figure legend, the reader is referred to the web version of this article.)

and the BE3 site overlaps with the indole ring of the co-crystallized ligand. The residues involving BE1 and BE3 sites were also found to be energetically important in the MM-GBSA analysis. The CSM analysis was also able to identify the transient non-native hydrogen bond observed in the MD simulation between the inhibitor and the amino acid residue R36, which overlapped with the AC2 cluster.

3.4. Hot spot analysis of efFabH

Mapping of the efFabH structure yielded seven hot spots within the substrate binding pocket (Fig. 5B). Docking methanol probes identified a hydrogen bond acceptor site interacting with residues N275 and H245 (OL1). Another hydrogen bond acceptor site making contact with residues R37 and R250 (AC1) was identified by docking acetate probes. A methyl ammonium probe populated cluster making contacts with the backbone of M213 (ME1) was classified as hydrogen bond donor consensus site. Docking benzene probes identified two aromatic consensus clusters, one making contacts with residues L189, I218, F221, A222, F307 and G308 (BE1); and the other making contacts with residues F219 and I251 (BE2). Docking ethane probes identified two hydrophobic consensus clusters near the base of the pocket. One cluster was found making contacts with residues I218, F221, A222, V226 and F307 (ET1). Another ethane populated cluster was found interacting with residues C112, F157, H245, F307 and G308 (ET2).

Three consensus sites identified in the CSM analysis overlap with the co-crystalized ligand in efFabH. The hydrogen bonding interaction involving H245 and N275 overlaps with the consensus site OL1. The interaction is also stable in the MD simulation and is predicted to contribute favorably to inhibitor binding in the energetic analysis. The hydrophobic interactions of the benzoic acid group of the ligand with residues I218, F221 and F307 superimpose well with the consensus site BE1. The third hot spot that overlaps with the bound ligand corresponds to the benzene populated cluster BE2 which superimpose with the ligand's benzoylamino group.

3.5. Comparison between ecFabH and efFabH hot spot maps

Despite high sequence and structural similarity between ecFabH and efFabH, we observed large differences in the favorable binding positions delineated by CSM. The two homologs share only three binding hot spots. The consensus site BE1 found by the mapping of the ecFabH structure overlaps with the consensus site BE1 of efFabH. This site interacts with the protein residues A216, L220, A246 and F304 in ecFabH and residues L189, I218, F221, A222, F307 and G308 in efFabH. The site also overlaps with the ecFabH and efFabH co-crystallized ligands. The second site shared by the two homologs is AC1 of ecFabH and AC1 of efFabH. This site interacts with the protein residue R36 in ecFabH and residues R37 and R250 in efFabH. The third site shared by the two homologs is ME2 of ecFabH and ME1 of efFabH which interacts with M207 in ecFabH and M213 in efFabH. All the common hot spots also show favorable contribution to the binding free energy in the two structures.

The potential origin of the differences in binding hot spots in ecFabH and efFabH can be explained by the distinct conformational preferences and the flexibility of the binding pocket residues in two homologs. At the base of the binding pocket, the side chains of the conserved residues L189, H244, I250 and F304 adopt different rotameric conformations in the two homologs (Fig. 3), resulting in the absence of hot spots equivalent to ecFabH ET1, BE2, ME1 and OL1 in the efFabH and conversely absence of hot spots equivalent to efFabH ET1, ET2 and OL1 in ecFabH. Previous studies have also suggested that by adopting different rotamers of F304, FabH can change the size of the CoA binding cleft across different species and hence modulate the enzyme's substrate specificity [14].

The CSM results differ significantly at the mouth of the binding pocket. These differences are predominantly due to greater dissimilarity in sequence and structural features. The residues comprising the mouth of the substrate binding pocket are poorly conserved between the two homologs, and the conserved residues exhibit different degrees of plasticity and preferred sidechain configurations. The steric hindrance due to the substitution of *E. coli* I156 to L156 and L248 toV249 along with high conformational flexibility of the conserved residue N247 led to the elimination of ecFabH site OL2 in efFabH. The different sidechain dihedral angle propensities of the conserved R36 (*E. coli*)/R37 (*E. faecalis*) in the two structures led to the elimination of ecFabH site AC2 in efFabH. The side chains of F213 and I250 adopt different configurations in the two structures, which led to the elimination of efFabH site BE2 in ecFabH. Conversely, ecFabH site BE3, which was also found to be energetically important for the binding of the crystallized ligand in ecFabH, did not map into efFabH. The mutation of *E. coli* I156 to L156 in *E. faecalis* and the higher conformational flexibility of W33 in efFabH led to the elimination of ecFabH site BE4 in efFabH.

4. Conclusions

In this study, we explored the conformational characteristics of FabH from a Gram-negative and a Gram-positive bacterium to identify the determinants of substrate and inhibitor specificity of FabH enzymes. We find that ecFabH and efFabH show significant differences in their equilibrium conformational ensembles and intrinsic fluctuations of the binding pocket residues, that complement the experimental data. It appears that the unique ligand binding properties of the two homologs stem from the distinct local conformational preferences of residues comprising the binding pocket. Using CSM analysis, we demonstrated that the two homologs show qualitatively different binding hot spots. The distinct rotameric preferences of several residues lead to steric restrictions and changes in the physico-chemical binding properties, due to which the small organic probes bind to differing sites in the two structures. The resulting differences in the binding of small molecules provide insight into why the two homologs show distinct ligand binding characteristics. More generally, these results highlight the need for improved computational approaches that account for conformational rearrangements of the receptor, for efficient design of inhibitors against FabH.

Acknowledgment

This work was supported in part by the US National Institutes of Health grant U01 AI077949.

Appendix A. Supplementary data

Supplementary data associated with this article can be found, in the online version, at http://dx.doi.org/10.1016/j.jmgm.2014.11.004.

References

[1] Y.-M. Zhang, C.O. Rock, Membrane lipid homeostasis in bacteria, Nat. Rev. Microbiol. 6 (2008) 222–233.
[2] S. Smith, The animal fatty acid synthase: one gene, one polypeptide, seven enzymes, FASEB J. 8 (1994) 1248–1259.
[3] A.J. Fulco, Fatty acid metabolism in bacteria, Prog. Lipid. Res. 22 (1983) 133–160.
[4] A.C. Price, K.-H. Choi, R.J. Heath, Z. Li, S.W. White, C.O. Rock, Inhibition of β-ketoacyl-acyl carrier protein synthases by thiolactomycin and cerulenin: structure and mechanism, J. Biol. Chem. 276 (2001) 6551–6559.
[5] J. Wang, S.M. Soisson, K. Young, W. Shoop, S. Kodali, A. Galgoci, et al., Platensimycin is a selective FabF inhibitor with potent antibiotic properties, Nature 441 (2006) 358–361.
[6] J. Wang, S. Kodali, S.H. Lee, A. Galgoci, R. Painter, K. Dorso, et al., Discovery of platencin, a dual FabF and FabH inhibitor with in vivo antibiotic properties, Proc. Natl. Acad. Sci. 104 (2007) 7612–7616.
[7] K. Young, H. Jayasuriya, J.G. Ondeyka, K. Herath, C. Zhang, S. Kodali, et al., Discovery of FabH/FabF inhibitors from natural products, Antimicrob. Agents Chemother. 50 (2006) 519–526.
[8] Y. Luo, Y.-S. Yang, J. Fu, H.-L. Zhu, Novel FabH inhibitors: a patent and article literature review (2000–2012), Expert Opin. Ther. Patents 22 (2012) 1325–1336.
[9] V. Gerusz, Chapter 18—recent advances in the inhibition of bacterial fatty acid biosynthesis, in: J.E. Macor (Ed.), Annual Reports in Medicinal Chemistry, vol. 45, Academic Press, San Diego, 2010, pp. 295–311.
[10] K.-H. Choi, R.J. Heath, C.O. Rock, β-Ketoacyl-acyl carrier protein synthase III (FabH) is a determining factor in branched-chain fatty acid biosynthesis, J. Bacteriol. 182 (2000) 365–370.
[11] Z. Nie, C. Perretta, J. Lu, Y. Su, S. Margosiak, K.S. Gajiwala, et al., Structure-based design, synthesis, and study of potent inhibitors of β-ketoacyl-acyl carrier protein synthase III as potential antimicrobial agents, J. Med. Chem. 48 (2005) 1596–1609.
[12] E.Z. Eisenmesser, D.A. Bosco, M. Akke, D. Kern, Enzyme dynamics during catalysis, Science 295 (2002) 1520–1523.
[13] S.-R. Tzeng, C.G. Kalodimos, Protein activity regulation by conformational entropy, Nature 488 (2012) 236–240.
[14] K.S. Gajiwala, S. Margosiak, J. Lu, J. Cortez, Y. Su, Z. Nie, et al., Crystal structures of bacterial FabH suggest a molecular basis for the substrate specificity of the enzyme, FEBS Lett. 583 (2009) 2939–2946.
[15] Y. Pérez-Castillo, M. Froeyen, M. Cabrera-Pérez, A. Nowé, Molecular dynamics and docking simulations as a proof of high flexibility in *E. coli* FabH and its relevance for accurate inhibitor modeling, J. Comput. Aided Mol. Des. 25 (2011) 371–393.
[16] T. Kortvelyesi, S. Dennis, M. Silberstein, L. Brown, S. Vajda, Algorithms for computational solvent mapping of proteins, Proteins: Struct. Funct. Bioinf. 51 (2003) 340–351.
[17] H.A. Carlson, K.M. Masukawa, J.A. McCammon, Method for including the dynamic fluctuations of a protein in computer-aided drug design, J. Phys. Chem. A 103 (1999) 10213–10219.
[18] H.A. Carlson, K.M. Masukawa, K. Rubins, F.D. Bushman, W.L. Jorgensen, R.D. Lins, et al., Developing a dynamic pharmacophore model for HIV-1 integrase, J. Med. Chem. 43 (2000) 2100–2114.
[19] R.A. Daines, I. Pendrak, K. Sham, G.S. Van Aller, A.K. Konstantinidis, J.T. Lonsdale, et al., First X-ray cocrystal structure of a bacterial FabH condensing enzyme and a small molecule inhibitor achieved using rational design and homology modeling, J. Med. Chem. 46 (2003) 5–8.
[20] D.A. Case, T.A. Darden, T.E. Cheatham, III, C.L. Simmerling, J. Wang, R.E. Duke, et al., AMBER10, University of California, San Francisco, CA, 2008.
[21] Y. Duan, C. Wu, S. Chowdhury, M.C. Lee, G. Xiong, W. Zhang, et al., A point-charge force field for molecular mechanics simulations of proteins based on condensed-phase quantum mechanical calculations, J. Comput. Chem. 24 (2003) 1999–2012.
[22] M. Feig, J. Karanicolas, C.L. Brooks III, MMTSB Tool Set: enhanced sampling and multiscale modeling methods for applications in structural biology, J. Mol. Graph. Model. 22 (2004) 377–395.
[23] G.M. Morris, D.S. Goodsell, R.S. Halliday, R. Huey, W.E. Hart, R.K. Belew, A.J. Olson, Automated docking using a Lamarckian genetic algorithm and empirical binding free energy function, J. Comput. Chem. 19 (1998) 1639–1662.
[24] H. Gohlke, D.A. Case, Converging free energy estimates: MM-PB(GB)SA studies on the protein–protein complex Ras–Raf, J. Comput. Chem. 25 (2004) 238–250.
[25] P.A. Kollman, I. Massova, C. Reyes, B. Kuhn, S. Huo, L. Chong, et al., Calculating structures and free energies of complex molecules: combining molecular mechanics and continuum models, Acc. Chem. Res. 33 (2000) 889–897.
[26] T. Hou, J. Wang, Y. Li, W. Wang, Assessing the performance of the MM/PBSA and MM/GBSA methods. 1. The accuracy of binding free energy calculations based on molecular dynamics simulations, J. Chem. Inf. Model. 51 (2011) 69–82.
[27] G. Rastelli, A.D. Rio, G. Degliesposti, M. Sgobba, Fast and accurate predictions of binding free energies using MM-PBSA and MM-GBSA, J. Comput. Chem. 31 (2010) 797–810.
[28] J. Zeng, W. Li, Y. Zhao, G. Liu, Y. Tang, H. Jiang, Insights into ligand selectivity in estrogen receptor isoforms: molecular dynamics simulations and binding free energy calculations, J. Phys. Chem. B 112 (2008) 2719–2726.
[29] J.D. Thompson, D.G. Higgins, T.J. Gibson, CLUSTAL W: improving the sensitivity of progressive multiple sequence alignment through sequence weighting, position-specific gap penalties and weight matrix choice, Nucleic Acids Res. 22 (1994) 4673–4680.
[30] M. Clamp, J. Cuff, S.M. Searle, G.J. Barton, The Jalview Java alignment editor, Bioinformatics 20 (2004) 426–427.
[31] A.M. Waterhouse, J.B. Procter, D.M.A. Martin, M. Clamp, G.J. Barton, Jalview version 2—a multiple sequence alignment editor and analysis workbench, Bioinformatics 25 (2009) 1189–1191.
[32] G.E. Crooks, G. Hon, J.-M. Chandonia, S.E. Brenner, WebLogo: a sequence logo generator, Genome Res. 14 (2004) 1188–1190.